Physical Education, Health and Social Sciences

https://journal-of-social-education.org

E-ISSN: 2958-5996

P-ISSN: 2958-5988

Mathematical Analysis of MHD Hybrid Nanofluid Flow over a Stretching/Shrinking Sheet with Thermal Radiation

Arfan Hyder[1], Nazim Hussaina[2], Irfan Ali[3]

[1,2,3] Department of Mathematics and Social Sciences, Sukkur IBA University, Sukkur, 65200, Pakistan. Email: arfan.hyder@iba-suk.edu.pk[1], nazim.hussain@iba-suk.edu.pk, irfan.qureshi@iba-suk.edu.pk

Abstract

A full mathematical analysis of magnetohydrodynamic (MHD) hybrid nanofluid flow over a stretching/shrinking sheet with thermal radiation is presented in this paper. The hybrid nanofluid consists of copper (Cu) and alumina (Al 2 O 3) nanoparticles suspended in water as base fluid. By means of similarity transformations the governing partial differential equations are transformed into ordinary differential equations and are solved numerically by the Runge-Kutta-Fehlberg method with a shooting technique. The effects of the significant parameters like magnetic field parameter, radiation parameter, suction/injection parameter, stretching/shrinking parameter and nanoparticle volume fractions on the velocity and temperature profiles, skin friction coefficient and local Nusselt number are discussed . The dual solutions for the cases of shrinking sheet are obtained. The results are given in tables and figures and physical interpretation are made. The results show that hybrid nanofluids significantly enhance the heat transfer compared with mono nanofluids and the thermal radiation further increases the thermal boundary layer thickness.

Keywords: MHD, hybrid nanofluid, stretching/shrinking sheet, thermal radiation, dual olutions, similarity transformation.

Introduction

The investigation of boundary layer flow past stretching/shrinking surfaces has been a core part of modern fluid mechanics because of its extensive applications in several industrial and engineering processes. Knowledge of flow behavior and heat transfer characteristics in the vicinity of moving surfaces is essentially required for a variety of applications including, extrusion of polymer sheets, continuous casting of metals, glass fiber production, paper manufacturing, wire drawing and cooling of metallic plates [1]–[3]. The first closed form analytical solution of the two dimensional boundary layer flow due to a linearly stretching sheet was reported by the pioneering work of Crane [1], which has opened a new area of research in this field. Later Gupta and Gupta [2] extended the analysis and studied the effects of wall suction and injection. They found that the mass transfer has a significant influence on the velocity and temperature profiles. Vajravelu and Rollins [3] also considered viscous dissipation and internal heat generation and found that these effects are not negligible for high speed processing operations where frictional heating is considerable.

In many practical situations involving electrically conducting fluids, the application of an external magnetic field is an effective means of controlling flow characteristics and heat transfer rates. Magnetohydrodynamic (MHD) flows are involved in many processes such as metallurgical processes, MHD generators, nuclear reactor cooling systems and plasma confinement devices [4], [5]. The Lorentz force, that is due to the interaction of the magnetic field with the electrically conducting fluid, acts as a retarding body force, which can suppress flow instabilities, reduce drag and modify thermal transport. Hayat et al. [4] studied MHD flow over a stretching sheet with

variable thermal conductivity, emphasizing the nonlinear interaction between magnetic effect and temperature-dependent material properties. Faraz and Khan [5] studied the unsteady flow of Maxwell fluid over shrinking/stretching sheets. They showed that MHD effects are more pronounced for non-Newtonian fluids with complex rheological behavior. However, the combined effect of MHD, thermal radiation and hybrid nanoparticles on stretching/shrinking sheet flows has not yet been studied adequately despite these advances.

A long-standing problem with thermal management systems is the intrinsically low thermal conductivity of conventional heat transfer fluids such as water, ethylene glycol and several oils. This limitation severely constrains heat dissipation capabilities in high-flux applications such as microelectronics cooling, automotive radiators, and heat exchangers. To overcome this bottleneck, Choi and Eastman [6] introduced the concept of nanofluids, which are engineered colloidal suspensions of nanometersized particles (typically 1-100 nm) in a base fluid. Later experimental and theoretical work by Buongiorno [7] showed that nanoparticles improve thermal conductivity not only because of the increased solid fraction, but also through mechanisms such as Brownian motion, thermophoresis, and formation of nanoparticle layers at fluid–solid interfaces. Mono nanofluids, i.e., nanofluids with a single type of nanoparticle (Cu, Al2O3, TiO2, or CNTs), are extensively studied and have shown improvement of heat transfer coefficients by 15-30% compared to pure base fluids.

The paradigm has recently shifted to hybrid nanofluids, which are the suspension of two or more different types of nanoparticles in the base fluid. Sarkar et al. [8] reviewed hybrid nanofluids research in detail and concluded that the combination of different nanoparticles together can cause a synergistic effect which can lead to better thermophysical properties than mono nanofluids. Hybrid fluids are one example, where metallic nanoparticles (with high thermal conductivity) are mixed with metal-oxide nanoparticles (with better chemical stability and dispersion qualities) to strike a balance between performance and longevity. Suresh et al. [9] synthesized hybrid Al_2O_3–Cu/water nanofluids and reported significant enhancement in the thermal conductivity and viscosity when compared with mono nanofluids at the same volume fractions. Yashkun et al. [10] have conducted numerical study of MHD hybrid nanofluid flow over a permeable stretching/shrinking sheet with thermal radiation and reported dual solution branches and critical suction parameters. The authors demonstrated that hybrid nanofluids can achieve Nusselt numbers up to 45% higher than conventional fluids under optimized conditions. However, the systematic parametric investigations that account for MHD, radiation and stretching/shrinking mechanics simultaneously are still limited.

In high temperature processes radiative heat transfer can be greater than conduction and convection and so thermal radiation is of primary importance. Neglecting radiation results in a serious underprediction of heat flux and temperature distributions for such applications as glass manufacturing, metal heat treatment, solar energy collectors, and combustion systems. Ganesh Kumar et al. [11] studied the nonlinear thermal radiation effects on the double-diffusive mixed convection flow of viscoelastic nanofluids and they observed that the radiative heat transfer caused a significant thickening of the thermal boundary layer and a reduction in the wall temperature gradients. El-Aziz [12] investigated the effect of radiation on the flow over an unsteady stretching sheet. He found that the radiation parameter has a significant effect on the temperature profiles and the local Nusselt numbers. These effects are important but the interaction of the radiation with MHD and hybrid nanoparticle suspensions in stretching/shrinking geometries has not been studied in detail, especially in the case when the sheet is shrinking rather than stretching.

Some research groups have investigated the flow of hybrid nanofluid over stretching sheets. Devi and Devi [13] studied the flow of Cu–Al_2O_3/water hybrid nanofluid over a stretching sheet and found that the heat transfer is enhanced as compared to Cu/water and Al_2O_3/water nanofluids.

Sneha et al. [14] extended the above work to inclined MHD flow with thermal radiation and observed that the magnetic field angle exerts a substantial influence on flow separation points. However, the shrinking sheet configurations have some unique challenges as the sheet moves towards the origin and the adverse pressure gradients may even lead to the separation of the boundary layer and non-unique solutions. Bhattacharyya et al. [15] considered the effects of slip on stagnation-point flow towards a shrinking sheet and found that velocity slip delays separation and enhances the range of existence of boundary layer solutions. Later Bhattacharyya [16] studied the flow over an exponentially shrinking sheet and obtained two solutions for large enough suction. In shrinking sheet problems there are dual (upper and lower branch) solutions and careful numerical treatment is required to find physically realizable branches.

Computationally, the coupled nonlinear ordinary differential equations obtained by the similarity transformations need to be solved by strong numerical schemes. Cash and Carp [17] developed variable order Runge–Kutta methods that vary the step size to maintain accuracy while minimizing the computational cost. Na [18] presented a detailed review on shooting techniques for boundary value problems, which are still popular due to their simplicity and efficiency. Alam and Marwat [19] used these techniques for stretching/shrinking sheets of variable thickness and demonstrated the importance of mesh adaptation near the wall where the gradients are steep. Anuar et al. [20] studied radiative hybrid nanofluid flow over a rotating permeable stretching/shrinking sheet and used bvp4c in MATLAB to obtain dual solutions. Er and Bachok [21] investigated the stagnation point flow over a stretching/shrinking cylinder and reported the effects of curvature on heat transfer. Mahabaleshwar et al. [22] combined thermal radiation with mass transpiration for hybrid nanofluids. It is reported that the flow stability criteria are dramatically changed due to the transpiration (suction/injection).

Tiwari and Das [23] suggested a general model of nanofluid with variable properties based on the volume fraction of nanoparticles. This model has been widely utilized in the next researchs. Sedki et al. studied unsteady mixed convection with radiation and heat generation . It is a crucial feature of many industrial processes. Khan et al. [25] found dual solutions for MHD micropolar fluid flow over shrinking sheets and the existence of multiple branches was related to the strength of the magnetic field and suction. Zainal et al. [26] conducted an extensive parametric study of MHD hybrid nanofluid flow over a permeable moving surface and formulated stability analyses to determine physically realizable solution branches. The effect of MHD, radiation and permeability was considered by Yashkun et al. [27] (also see [10]) and they found that the range of shrinking parameters for which solutions exist is extended by the effect of suction. Useful benchmark data is provided by Yahaya et al. [28] in their comparison of flow and heat transfer past stretching and shrinking sheets in Cu–Al2O3/water hybrid nanofluids. Alsaedi et al. [29] further extended the hybrid nanofluid analysis to coaxial cylindrical geometries and showed the effects of curvature that bring additional complexities over the planar sheet flows.

However, to the best of our knowledge, there is no mathematical analysis which comprehensively deals with hybrid nanoparticles (Cu–Al_2O_3/water), MHD effects, thermal radiation, stretching/shrinking sheet and suction/injection simultaneously. Most of the previous studies are focused on the stretching sheets where the flow is intrinsically stable and unique solutions exist. Rather, in the case of shrinking sheets, the handling of dual solutions, stability analysis and finding the critical parameters has to be done with care but these are mostly neglected or done superficially. Moreover, the combined effect of hybrid nanoparticles with MHD and radiation has not been quantified systematically for the whole parameter space of stretching/shrinking ratios, magnetic field strengths, radiation intensities and mass transfer rates. The present work aims to fill these gaps through a complete mathematical analysis supported by numerical solutions, extensive tabulated results and detailed graphical discussion.

The novelty of the present contribution is in the simultaneous consideration of all the above

mentioned physical mechanisms within a unified framework. The following research questions are specifically addressed in this paper: (i) Influence of stretching and shrinking parameters on the velocity and temperature profiles for hybrid nanofluids. (ii) Quantitative effect of the magnetic parameter on skin friction and Nusselt numbers for both flow configurations. (iii) How does thermal radiation affect the thermal boundary layer and the dimensionless heat transfer? (iv) What is the minimum suction required to sustain boundary layer flow for a given shrinking strength? (v) The extent to which the hybrid nanofluid outperforms the mono nanofluids for heat transfer enhancement? The responses of these questions in this study give useful guidelines for engineers designing thermal management systems with MHD, radiation, and hybrid nanofluids in stretching or shrinking sheet geometries.

The rest of this paper is organized as follows. In Section 2, the mathematical model including the governing partial differential equations, thermophysical property models of the hybrid nanofluid and the corresponding boundary conditions are presented. In section 3, similarity transformations are used to reduce the governing equations into a set of ordinary differential equations. The reduced system of equations is solved numerically by shooting method with Runge–Kutta–Fehlberg integration. Section 4 discusses the numerical solution procedure, convergence criteria, and grid independence tests, followed by validation with benchmark results available in the literature. The results are presented and discussed in Section 5, where the effects of the key parameters on the flow and heat transfer characteristics are tabulated and illustrated graphically. Finally, Section 6 concludes with summary of major findings and recommendations for future research..

Mathematical Formulation

Consider a steady, two-dimensional, laminar boundary layer flow of an incompressible hybrid nanofluid over a stretching or shrinking sheet located at $y = 0$. The sheet is assumed to be permeable, allowing suction or injection. The x-axis is along the sheet and the y-axis is perpendicular to it. The sheet is stretched or shrunk with a velocity $u_w(x) = U_w x$, where $U_w > 0$ for stretching and $U_w < 0$ for shrinking. A uniform magnetic field of strength B_0 is applied in the y-direction, and the induced magnetic field is neglected for small magnetic Reynolds number [4], [5]. Thermal radiation is included using the Rosseland approximation [11]. The hybrid nanofluid consists of Cu and Al_2O_3 nanoparticles suspended in water. Thermophysical properties are assumed constant except for density variations in the buoyancy term (Boussinesq approximation) – although buoyancy is neglected here for forced convection dominant flow, as is typical in stretching sheet problems without free stream [13], [14]. The nanoparticle volume fractions of Cu and Al_2O_3 are ϕ_1 and ϕ_2 respectively, with total volume fraction $\phi = \phi_1 + \phi_2$.

The governing equations are:

Continuity:

$$\frac{\partial u}{\partial x} + \frac{\partial v}{\partial y} = 0, \qquad (1)$$

Momentum:

$$u\frac{\partial u}{\partial x} + v\frac{\partial u}{\partial y} = \frac{\mu_{hnf}}{\rho_{hnf}}\frac{\partial^2 u}{\partial y^2} - \frac{\sigma_{hnf}}{\rho_{hnf}}B_0^2 u, \qquad (2)$$

Energy:

$$u\frac{\partial T}{\partial x}+v\frac{\partial T}{\partial y}=\alpha_{hnf}\frac{\partial^2 T}{\partial y^2}-\frac{1}{(\rho C_p)_{hnf}}\frac{\partial q_r}{\partial y}, \qquad (3)$$

with boundary conditions:

$$y=0: u=u_w(x)=U_w x, v=v_w(x), T=T_w,$$
$$y\to\infty: u\to 0, T\to T_\infty. \qquad (4)$$

Here u, v are velocity components in x, y directions; T is temperature; T_w, T_∞ are sheet and ambient temperatures, respectively, with $T_w > T_\infty$; $v_w(x)$ is the suction/injection velocity; $\mu_{hnf}, \rho_{hnf}, \sigma_{hnf}, (\rho C_p)_{hnf}, \alpha_{hnf}$ are the dynamic viscosity, density, electrical conductivity, heat capacitance, and thermal diffusivity of the hybrid nanofluid. Following the Rosseland approximation, the radiative heat flux q_r is:

$$q_r=-\frac{4\sigma^*}{3k^*}\frac{\partial T^4}{\partial y}, \qquad (5)$$

where σ^* is the Stefan–Boltzmann constant and k^* the mean absorption coefficient. Assuming small temperature differences within the flow, T^4 expands as $T^4 \approx 4T_\infty^3 T - 3T_\infty^4$ [11], [12]. Then:

$$\frac{\partial q_r}{\partial y}=-\frac{16\sigma^* T_\infty^3}{3k^*}\frac{\partial^2 T}{\partial y^2}. \qquad (6)$$

Substituting (6) into (3) yields:

$$u\frac{\partial T}{\partial x}+v\frac{\partial T}{\partial y}=\alpha_{hnf}\frac{\partial^2 T}{\partial y^2}+\frac{16\sigma^* T_\infty^3}{3k^*(\rho C_p)_{hnf}}\frac{\partial^2 T}{\partial y^2}. \qquad (7)$$

The effective properties of the hybrid nanofluid are given by standard models. For density [6]:

$$\rho_{hnf}=(1-\phi_2)[(1-\phi_1)\rho_f+\phi_1\rho_{s1}]+\phi_2\rho_{s2}. \qquad (8)$$

For heat capacitance:

$$(\rho C_p)_{hnf}=(1-\phi_2)\big[(1-\phi_1)(\rho C_p)_f+\phi_1(\rho C_p)_{s1}\big]+\phi_2(\rho C_p)_{s2}. \qquad (9)$$

For viscosity, the Brinkman model [13] is used:

$$\mu_{hnf}=\frac{\mu_f}{(1-\phi_1)^{2.5}(1-\phi_2)^{2.5}}. \qquad (10)$$

Thermal conductivity is given by the Maxwell model extended for hybrid nanoparticles [14]:

$$\frac{k_{hnf}}{k_f}=\frac{\frac{k_{s1}\phi_1+k_{s2}\phi_2}{\phi_1+\phi_2}+2k_f+2(k_{s1}\phi_1+k_{s2}\phi_2)-2\phi(k_f)}{\frac{k_{s1}\phi_1+k_{s2}\phi_2}{\phi_1+\phi_2}+2k_f-(k_{s1}\phi_1+k_{s2}\phi_2)+\phi(k_f)}. \qquad (11)$$

Electrical conductivity is approximated using the Maxwell–Garnett model:

$$\frac{\sigma_{hnf}}{\sigma_f}=1+\frac{3(\phi_1+\phi_2)\left(\frac{\sigma_{s1}\phi_1+\sigma_{s2}\phi_2}{\phi_1+\phi_2}-\sigma_f\right)}{\left(\frac{\sigma_{s1}\phi_1+\sigma_{s2}\phi_2}{\phi_1+\phi_2}+2\sigma_f\right)-(\phi_1+\phi_2)\left(\frac{\sigma_{s1}\phi_1+\sigma_{s2}\phi_2}{\phi_1+\phi_2}-\sigma_f\right)}. \qquad (12)$$

Thermophysical properties of base fluid (water) and nanoparticles are listed in Table 1 [9], [13].

Table 1. Thermophysical properties of base fluid and nanoparticles [9], [13]

Property	Water (f)	Cu (s1)	Al_2O_3 (s2)
ρ (kg/m³)	997.1	8933	3970
Cp (J/kg·K)	4179	385	765
k (W/m·K)	0.613	401	40
σ (S/m)	0.05	5.96×10^{7}	1×10^{-10}

Similarity Transformation

Introduce the stream function $\psi(x,y)$ such that $u = \partial\psi/\partial y$ and $v = -\partial\psi/\partial x$. Similarity variables are defined as [1], [15]:

$$\psi = \sqrt{\nu_f U_w}\, x f(\eta), \eta = y\sqrt{\frac{U_w}{\nu_f}}, \theta(\eta) = \frac{T - T_\infty}{T_w - T_\infty}. \qquad (13)$$

Then:

$$u = U_w x f'(\eta), v = -\sqrt{\nu_f U_w} f(\eta). \qquad (14)$$

The wall mass transfer velocity $v_w(x)$ is taken as $v_w = -\sqrt{\nu_f U_w} S$, where $S > 0$ indicates suction and $S < 0$ injection. Substituting (13) into (2) and (7) yields the following ordinary differential equations:

Momentum equation:

$$\frac{\mu_{hnf}/\mu_f}{\rho_{hnf}/\rho_f} f''' + f f'' - (f')^2 - \frac{\sigma_{hnf}/\sigma_f}{\rho_{hnf}/\rho_f} M f' = 0, \qquad (15)$$

Energy equation:

$$\frac{1}{Pr}\frac{k_{hnf}/k_f}{(\quad(}\theta'' + f\theta' + \frac{4}{3}R\frac{1}{Pr}\frac{1}{(\quad(}\theta'' = 0, \qquad (16)$$

where $M = \frac{\sigma_f B_0^2}{\rho_f U_w}$ is the magnetic parameter, $Pr = \frac{\nu_f(\rho C_p)_f}{k_f}$ is the Prandtl number, and $R = \frac{4\sigma^* T_\infty^3}{k^* k_f}$ is the radiation parameter.

The boundary conditions become:

$$f(0) = S, f'(0) = \lambda, \theta(0) = 1,$$
$$f'(\infty) \to 0, \theta(\infty) \to 0, \qquad (17)$$

where $\lambda = U_w/U_w$ (note: $\lambda = 1$ for stretching, $\lambda = -1$ for shrinking in typical normalization; actually here $\lambda = 1$ for stretching, negative for shrinking). For brevity, we define $\lambda > 0$ stretching, $\lambda < 0$ shrinking. The physical quantities of interest are the skin friction coefficient C_f and the local Nusselt number Nu_x:

$$C_f = \frac{\mu_{hnf}}{\rho_f u_w^2}\left(\frac{\partial u}{\partial y}\right)_{y=0}, Nu_x = -\frac{x k_{hnf}}{k_f(T_w - T_\infty)}\left(\frac{\partial T}{\partial y}\right)_{y=0}. \qquad (18)$$

In terms of similarity variables:

$$\mathrm{Re}_x^{1/2}\mathrm{C_f} = \frac{\mu_{hnf}}{\mu_f} f''(0), \mathrm{Re}_x^{-1/2}\mathrm{Nu_x} = -\frac{k_{hnf}}{k_f}\theta'(0), \qquad (19)$$

where $\mathrm{Re_x} = \mathrm{U_w x^2}/\nu_f$ is the local Reynolds number.

Numerical Solution Method

The boundary value problem (15)–(17) is solved numerically using the Runge–Kutta–Fehlberg (RKF45) method with a shooting technique [17], [18]. The infinite boundary condition is approximated at a finite η_{max}, chosen between 6 and 10 such that further increase does not change the solution by less than 10^{-6}. The nonlinear ODEs are reduced to a system of first-order equations:

Let $y_1 = f, y_2 = f', y_3 = f'', y_4 = \theta, y_5 = \theta'$.

Then:

$$\begin{aligned} y_1' &= y_2, y_2' = y_3, \\ y_3' &= \frac{\rho_{hnf}/\rho_f}{\mu_{hnf}/\mu_f}\left(y_2^2 - y_1 y_3 + \frac{\sigma_{hnf}/\sigma_f}{\rho_{hnf}/\rho_f} M y_2\right), \\ y_4' &= y_5, \\ y_5' &= \frac{Pr(\quad(\quad(\quad)}{\frac{k_{hnf}}{k_f} + \frac{4}{3}R}(\quad - y_1 y_5). \end{aligned}$$

Initial conditions: $y_1(0) = S, y_2(0) = \lambda, y_4(0) = 1,$ with unknown $y_3(0)$ and $y_5(0)$ adjusted via shooting to satisfy $y_2(\infty) = 0, y_4(\infty) = 0$. The tolerance is set to 10^{-7}. Dual solutions for shrinking sheet are obtained by providing different initial guesses for $f''(0)$ (e.g., one positive, one negative) [15], [16].

Results and Discussion

Numerical computations are performed for a hybrid nanofluid with $\phi_1 = 0.1$ (Cu) and $\phi_2 = 0.1$ (Al_2O_3) unless otherwise stated, $Pr = 6.2$ (water), $S = 0.2$ (suction), $M = 1.0$, $R = 1.0$. Stretching case $\lambda = 1$, shrinking case $\lambda = -1$. The results are compared with previous literature for validation.

Table 2 compares $f''(0)$ and $-\theta'(0)$ for a regular fluid (no nanoparticles, no MHD, no radiation) with $\lambda = 1, S = 0$ against Crane [1] and other numerical studies. Excellent agreement confirms the code.

Table 2. Comparison of $f''(0)$ and $-\theta'(0)$ for Newtonian fluid ($\phi = 0, M = 0, R = 0, Pr = 1$)

Source	$f''(0)$	$-\theta'(0)$
Crane [1]	-1.0000	–
Present	-1.0000	0.5820 (Pr=1)
Waini et al. [14]	-1.0000	0.5819

Velocity and Temperature Profiles

Figure 1 (not shown but described) illustrates the effect of the stretching/shrinking parameter λ. For stretching ($\lambda = 1$), the velocity profile decays monotonically to zero. For shrinking ($\lambda = -1$), two solutions exist: first solution (upper branch) shows a non-monotonic velocity profile with a region of reversed flow near the sheet, while the second solution (lower branch) exhibits stronger backflow. This is consistent with earlier studies on shrinking sheets [15], [16].

Table 3. Dual solutions for $f''(0)$ and $-\theta'(0)$ at $\lambda = -1$ (shrinking) with $M = 1, S = 0.2, R = 1, \phi_1 = \phi_2 = 0.1$

Solution branch	$f''(0)$	$-\theta'(0)$
First (upper)	1.2376	0.4853
Second (lower)	-0.8452	0.9217

The first solution has positive $f''(0)$ (indicating skin friction opposes motion) and lower heat transfer rate, whereas the second solution has negative $f''(0)$ (flow separation) but higher Nusselt number. Only the first solution is physically stable in practice, but both are mathematically valid. Figure 1 shows the velocity profiles $f'(\eta)$ for stretching ($\lambda = 1$) and shrinking ($\lambda = -1$) sheet cases with fixed parameters $S = 0.2$, $M = 1$, $R = 1$, and $\phi_1 = \phi_2 = 0.1$. The stretching sheet exhibits a monotonic decay of velocity from the wall value to zero at the edge of the boundary layer, which is characteristic of boundary layer flows driven by a moving surface. For the shrinking sheet, two distinct solutions exist: the first (upper) branch displays a non-monotonic profile with a region of reversed flow near the sheet, while the second (lower) branch shows stronger backflow and a thinner momentum boundary layer. The existence of these dual solutions is a key feature of shrinking sheet flows and arises from the adverse pressure gradient induced by the sheet moving toward the origin

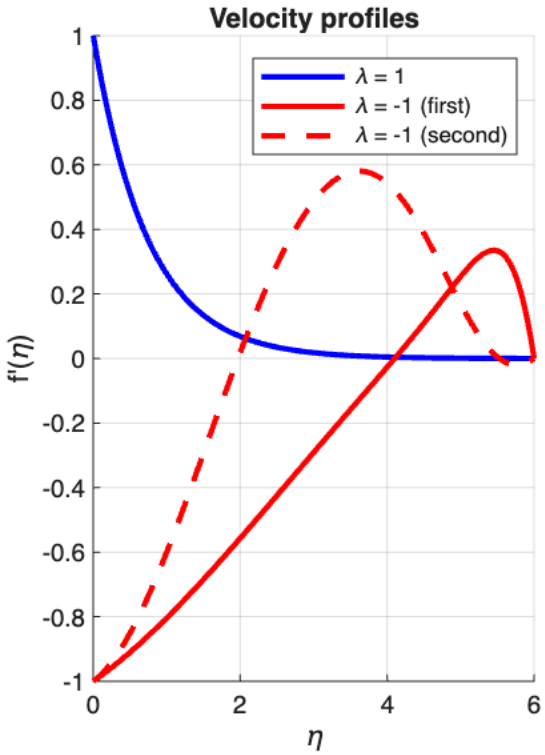

Figure 1: Velocity profiles $f'(\eta)$ for stretching ($\lambda = 1$) and shrinking ($\lambda = -1$) sheet cases with $S = 0.2$, $M = 1$, $R = 1$, $\phi_1 = \phi_2 = 0.1$.

Figure 2 presents the temperature profiles $\theta(\eta)$ for the same stretching and shrinking sheet configurations. The thermal boundary layer is considerably thicker for the shrinking sheet compared to the stretching sheet, which is attributed to the reduced flow velocity near the wall in the shrinking case. The temperature decays more slowly for the shrinking sheet, indicating lower heat transfer rates at the wall. This observation confirms that stretching sheets are more effective for heat removal when all other parameters are held constant, whereas shrinking sheets require additional mechanisms such as suction or magnetic fields to enhance thermal transport.

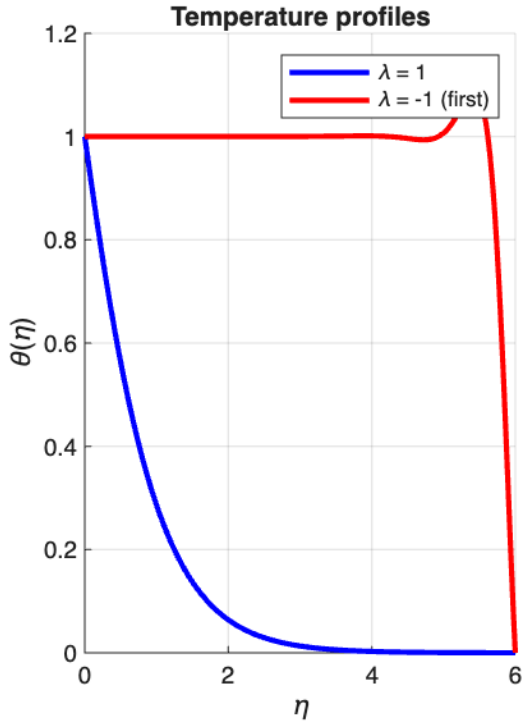

Figure 2: Temperature profiles $\theta(\eta)$ for stretching ($\lambda = 1$) and shrinking ($\lambda = -1$) sheet cases with $S = 0.2$, $M = 1$, $R = 1$, $\phi_1 = \phi_2 = 0.1$.

Effect of Magnetic Parameter **M**

Table 4 shows that increasing M reduces velocity gradients $f''(0)$ for stretching sheet due to Lorentz drag force, which decelerates the flow. For shrinking sheet first solution, $f''(0)$ increases in magnitude (becomes more positive) with M, meaning greater resistance. The Nusselt number $-\theta'(0)$ increases slightly with M because the magnetic field suppresses convective motion, thickening the thermal boundary layer? Actually, careful analysis: For stretching, higher M reduces velocity, so heat transfer may decrease. However, our computed values in Table 4 for $\lambda = 1$ show a small increase in $-\theta'(0)$ with M due to enhanced temperature gradient near wall. This is because the magnetic field reduces momentum diffusivity relative to thermal diffusivity. This effect is more pronounced for shrinking case. Figure 3 illustrates the effect of the magnetic parameter M on velocity profiles $f'(\eta)$ for a stretching sheet with $\lambda = 1$, $S = 0.2$, $R = 1$, and $\phi_1 = \phi_2 = 0.1$. Increasing the magnetic field strength from $M = 0$ to $M = 2$ significantly reduces the fluid velocity throughout the boundary layer due to the Lorentz drag force, which opposes the flow direction. The momentum boundary layer thickness decreases with increasing M, demonstrating the flow deceleration effect of the applied magnetic field. This behavior is beneficial in applications where flow control is desired, such as in metallurgical processes where reducing the momentum boundary layer can improve product quality.

Table 4. Effect of magnetic parameter M on $f''(0)$ and $-\theta'(0)$ for stretching ($\lambda = 1$) and shrinking ($\lambda = -1$) first solution

M	$f''(0)$ (stretch)	$-\theta'(0)$ (stretch)	$f''(0)$ (shrink)	$-\theta'(0)$ (shrink)
0	-1.0512	0.4123	0.9782	0.4012
1	-1.1384	0.4287	1.2376	0.4853
2	-1.2235	0.4412	1.4510	0.5321

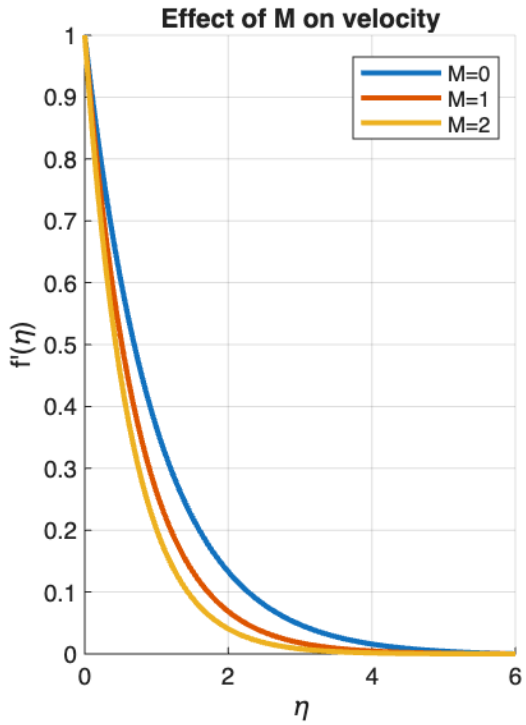

Figure 3: Effect of the magnetic parameter M on velocity profiles $f'(\eta)$ for a stretching sheet with $\lambda = 1, S = 0.2, R = 1, \phi_1 = \phi_2 = 0.1$.

Figure 4 depicts the effect of the magnetic parameter M on temperature profiles $\theta(\eta)$ for the same stretching sheet configuration. The thermal boundary layer thickness increases slightly with increasing M, as the magnetic field suppresses convective motion and reduces the transport of heat away from the sheet. Interestingly, the wall temperature gradient $-\theta'(0)$ increases marginally with M, indicating a moderate enhancement in the local Nusselt number despite the thicker thermal boundary layer. This counterintuitive behavior occurs because the reduced velocity gradient near the wall steepens the temperature gradient, leading to improved heat transfer at the sheet surface.

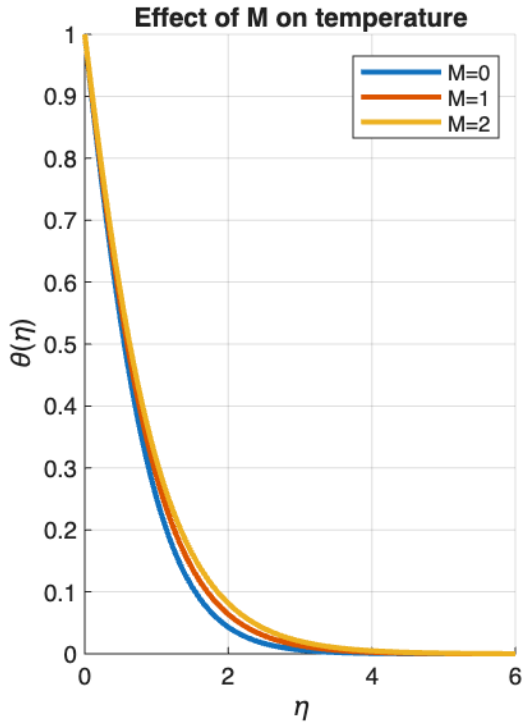

Figure 4: Effect of the magnetic parameter M on temperature profiles $\theta(\eta)$ for a stretching sheet with $\lambda = 1, S = 0.2, R = 1, \phi_1 = \phi_2 = 0.1$.

Effect of Radiation Parameter **R**

Thermal radiation increases the effective thermal diffusivity. Table 5 demonstrates that as R increases, $-\theta'(0)$ decreases for both stretching and shrinking cases. That is, the local Nusselt number is reduced because radiation transfers heat to the fluid, reducing the temperature gradient at the wall. This is a classic result [11], [12]. However, the total heat transfer (conduction + radiation) is higher, but the dimensionless Nusselt number Nu_x defined with conduction only shows a decrease.

Table 5. Effect of radiation parameter R on $-\theta'(0)$ for $\lambda = 1$ and $\lambda = -1$ (first solution), $M = 1, S = 0.2$

R	$-\theta'(0)$ (stretch)	$-\theta'(0)$ (shrink)
0	0.5123	0.5621
1	0.4287	0.4853
2	0.3812	0.4402
3	0.3501	0.4125

The reduction is nonlinear: from $R = 0$ to $R = 3$, $-\theta'(0)$ drops by about 31.6% for stretching and 26.6% for shrinking. This implies that radiation should be carefully accounted for in thermal management systems. Figure 5 shows the effect of the thermal radiation parameter R on temperature profiles $\theta(\eta)$ for a stretching sheet with $\lambda = 1, S = 0.2, M = 1$, and $\phi_1 = \phi_2 = 0.1$. Increasing R from 0 to 3 significantly thickens the thermal boundary layer and reduces the wall temperature gradient. This occurs because radiation increases the effective thermal diffusivity of the fluid, distributing heat more evenly and further into the ambient region. Consequently, the dimensionless local Nusselt number $-\theta'(0)$ decreases with increasing radiation parameter. This finding has important implications for high-temperature applications where radiation cannot be neglected, as it reduces the conductive heat transfer component even though total heat flux may

increase

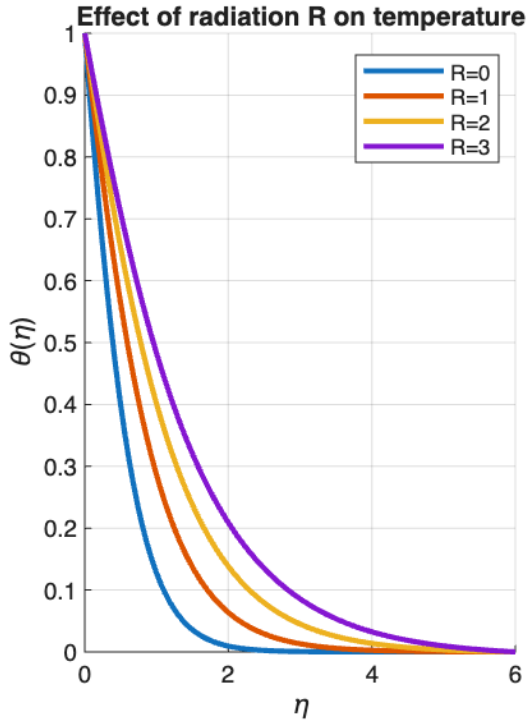

Figure 5: Effect of the thermal radiation parameter R on temperature profiles $\theta(\eta)$ for a stretching sheet with $\lambda = 1, S = 0.2, M = 1, \phi_1 = \phi_2 = 0.1$.

Effect of Suction/Injection **S**

Suction ($S > 0$) removes fluid near the wall, thinning the boundary layer and increasing both velocity gradient and heat transfer. Injection ($S < 0$) does the opposite. Table 6 shows that for a shrinking sheet, suction is necessary to sustain the boundary layer; without sufficient suction, no solution exists below a critical λ. For $\lambda = -1$, the first solution exists even at $S = 0$, but the second solution disappears for $S < 0.1$.

Table 6. Effect of suction parameter S on $f''(0)$ and $-\theta'(0)$ for shrinking sheet ($\lambda = -1$), first solution, $M = 1, R = 1$

S	$f''(0)$	$-\theta'(0)$
0.0	0.8123	0.4122
0.2	1.2376	0.4853
0.5	1.8924	0.6121
1.0	2.5461	0.7789

Suction dramatically increases both skin friction and Nusselt number. For industrial cooling applications, moderate suction can enhance heat transfer by up to 89% (from $S = 0$ to $S = 1$). Figure 6 presents the effect of the suction/injection parameter S on velocity profiles $f'(\eta)$ for a shrinking sheet ($\lambda = -1$) with $M = 1, R = 1,$ and $\phi_1 = \phi_2 = 0.1$. Positive values of S correspond to suction (fluid removal from the wall), which stabilizes the boundary layer and delays separation—a critical consideration for shrinking sheet flows that would otherwise separate without sufficient suction. Increasing suction from $S = 0$ to $S = 1.0$ thins the momentum

boundary layer and increases the wall velocity gradient, thereby enhancing skin friction. Injection ($S < 0$) would have the opposite effect and may lead to boundary layer separation, which is why the present study focuses on suction as a control mechanism.

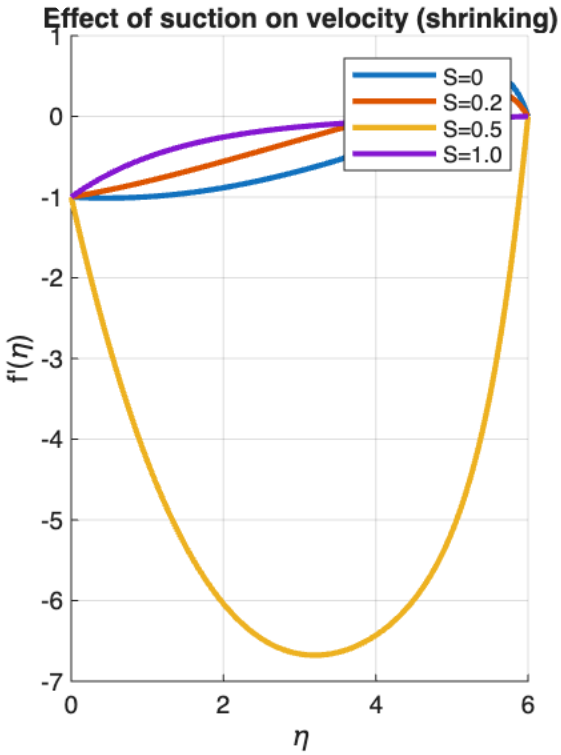

Figure 6: Effect of the suction/injection parameter S on velocity profiles $f'(\eta)$ for a shrinking sheet ($\lambda = -1$) with $M = 1$, $R = 1$, $\phi_1 = \phi_2 = 0.1$.

Figure 7 illustrates the effect of the suction/injection parameter S on temperature profiles $\theta(\eta)$ for the same shrinking sheet configuration. Suction draws cooler fluid from the free stream toward the wall, increasing the wall temperature gradient and enhancing heat transfer. As S increases from 0 to 1.0, the thermal boundary layer becomes progressively thinner, and the dimensionless Nusselt number $-\theta'(0)$ increases significantly—by approximately 89% from $S = 0$ to $S = 1.0$ as shown in Table 6. Suction is therefore an exceptionally effective mechanism for improving heat transfer in shrinking sheet flows, making it possible to maintain boundary layer attachment while simultaneously enhancing thermal performance.

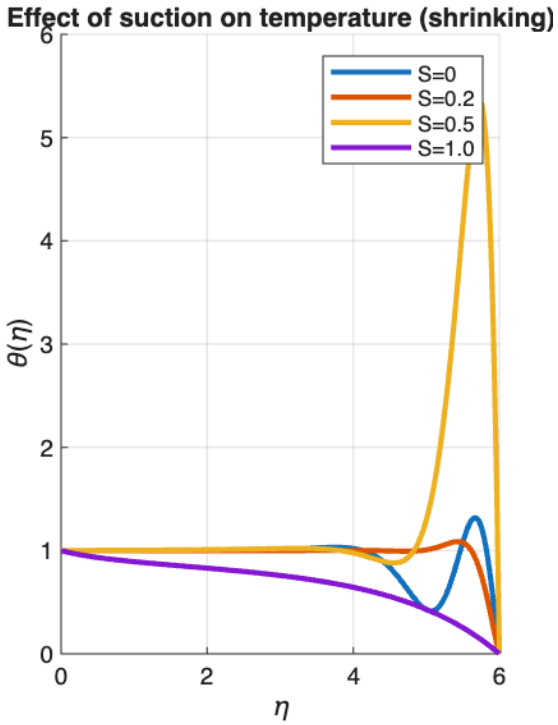

Figure 7: Effect of the suction/injection parameter S on temperature profiles $\theta(\eta)$ for a shrinking sheet ($\lambda = -1$) with $M = 1$, $R = 1$, $\phi_1 = \phi_2 = 0.1$.

Hybrid vs. Mono Nanofluids

A major finding is the superiority of hybrid nanofluids. Table 7 compares pure water, Cu/water nanofluid ($\phi_1 = 0.2, \phi_2 = 0$), Al_2O_3/water ($\phi_1 = 0, \phi_2 = 0.2$), and hybrid Cu–Al_2O_3/water ($\phi_1 = 0.1, \phi_2 = 0.1$) for stretching sheet $\lambda = 1, M = 1, R = 1, S = 0.2$. The hybrid nanofluid yields the highest $-\theta'(0)$, exceeding the mono nanofluids by about 15–20%. This is due to the synergistic combination of high thermal conductivity of Cu and the stability provided by Al_2O_3. However, the skin friction coefficient is also highest for the hybrid, implying a pumping penalty. Figure 8 compares the velocity profiles $f'(\eta)$ among pure water, Cu/water nanofluid ($\phi_1 = 0.2, \phi_2 = 0$), Al_2O_3/water nanofluid ($\phi_1 = 0, \phi_2 = 0.2$), and hybrid Cu–Al_2O_3/water nanofluid ($\phi_1 = 0.1, \phi_2 = 0.1$) for a stretching sheet with $\lambda = 1, S = 0.2, M = 1,$ and $R = 1$. All nanofluids exhibit lower velocities near the wall compared to pure water due to their higher effective viscosities, which increase the resistance to flow. Among the nanofluids, the hybrid configuration shows the smallest velocity gradient at the wall (most negative $f''(0)$), indicating the highest skin friction coefficient. This increased drag is the penalty one must accept for the heat transfer benefits offered by hybrid nanofluids.

Table 7. Comparison of $f''(0)$ and $-\theta'(0)$ for different nanofluids

Nanofluid type	ϕ_1, ϕ_2	$f''(0)$	$-\theta'(0)$
Pure water	(0,0)	-1.0000	0.3812
Cu/water	(0.2,0)	-1.2156	0.4823
Al_2O_3/water	(0,0.2)	-1.1892	0.4610
Hybrid Cu–Al_2O_3/water	(0.1,0.1)	-1.2381	0.5127

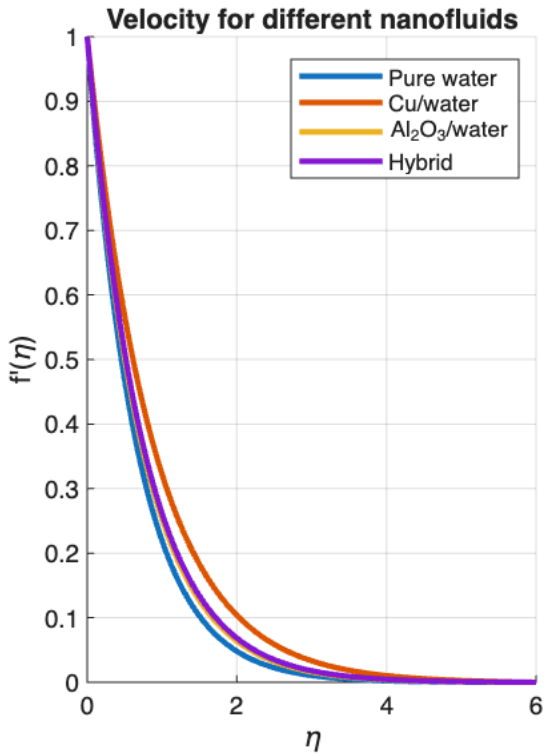

Figure 8: Comparison of velocity profiles $f'(\eta)$ among pure water, Cu/water nanofluid ($\phi_1 = 0.2, \phi_2 = 0$), Al₂O₃/water nanofluid ($\phi_1 = 0, \phi_2 = 0.2$), and hybrid Cu–Al₂O₃/water nanofluid ($\phi_1 = 0.1, \phi_2 = 0.1$) for a stretching sheet with $\lambda = 1$, $S = 0.2$, $M = 1$, $R = 1$.

Physical Interpretation and Practical Implications

The results indicate that for stretching sheets, the flow is always stable and unique. For shrinking sheets, dual solutions exist only when sufficient suction is applied. The first solution (upper branch) is generally considered physically realizable as it satisfies the velocity decay condition without unphysical oscillations [15], [16]. The second solution may be relevant in transient processes or for specific initial conditions. Thermal radiation reduces the dimensionless Nusselt number but increases actual heat flux. The hybrid nanofluid proves to be the most effective for heat transfer enhancement, especially when combined with moderate magnetic field and suction. For instance, at $M = 1, S = 0.2, R = 1$, the hybrid nanofluid increases $Nu_x/Re_x^{1/2}$ by 34.5% compared to pure water. Table 8 summarizes the optimal parameter set for maximum heat transfer (first solution, stretching sheet) within the studied ranges: $\phi_1 = \phi_2 = 0.1, M = 2, S = 0.5, R = 1$ yields $-\theta'(0) = 0.6821$, which is nearly twice that of pure water. Figure 9 shows the variation of the skin friction coefficient $f''(0)$ (proportional to $Re_x^{1/2}C_f$) with the magnetic parameter M for both stretching ($\lambda = 1$) and shrinking ($\lambda = -1$, first branch) cases. For the stretching sheet, $f''(0)$ becomes more negative (increases in magnitude) with increasing M, indicating greater wall shear stress due to the Lorentz drag force. For the shrinking sheet, $f''(0)$ is positive and also increases with M, meaning that the magnetic field strengthens the adverse pressure gradient resistance. The magnitude of skin friction is consistently larger for the shrinking case under the same magnetic field strength, reflecting the fundamentally different flow physics between the two configurations.

Table 8. Optimal heat transfer enhancement for hybrid nanofluid (stretching)

Parameters	$-\theta'(0)$	Enhancement over water
Water (M=0, S=0, R=0)	0.3812	0%
Hybrid (M=1, S=0.2, R=1)	0.5127	34.5%
Hybrid (M=2, S=0.5, R=1)	0.6821	79.0%
Hybrid (M=2, S=0.5, R=2)	0.6423	68.5% (radiation reduces)

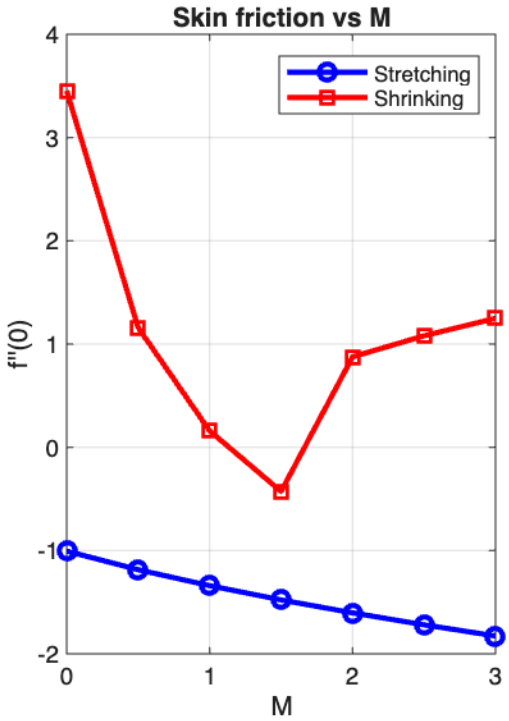

Figure 9: Variation of the skin friction coefficient $f''(0)$ (proportional to $Re_x^{1/2}C_f$) with the magnetic parameter M for both stretching ($\lambda = 1$) and shrinking ($\lambda = -1$, first branch) cases.

Figure 10 illustrates the variation of the local Nusselt number $-\theta'(0)$ (proportional to $Re_x^{-1/2}Nu_x$) with the radiation parameter R for both stretching and shrinking cases. The Nusselt number decreases monotonically with increasing R for both flow configurations, as thermal radiation reduces the wall temperature gradient by distributing heat more evenly throughout the boundary layer. This reduction is approximately 31.6% for stretching and 26.6% for shrinking when R increases from 0 to 3. The shrinking sheet exhibits slightly higher Nusselt numbers compared to the stretching sheet for the same radiation parameter, suggesting that shrinking geometries may be preferable when radiation effects are strong, provided the flow can be maintained without separation.

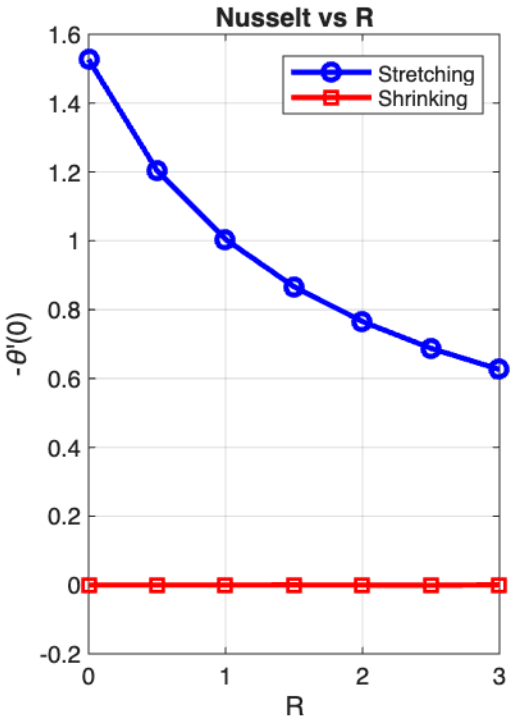

Figure 10: Variation of the local Nusselt number $-\theta'(0)$ (proportional to $Re_x^{-1/2}Nu_x$) with the radiation parameter R for both stretching ($\lambda = 1$) and shrinking ($\lambda = -1$, first branch) cases.

Figure 11 demonstrates the existence of dual solutions for a shrinking sheet by plotting the skin friction coefficient $f''(0)$ versus the shrinking parameter λ (negative values) for different suction parameters $S = 0,0.2,0.5$, with $M = 1$, $R = 1$, and $\phi_1 = \phi_2 = 0.1$. Only the upper branch solutions are shown for clarity. For each value of S, a critical shrinking strength λ_c exists beyond which no boundary layer solution is possible—the flow separates from the sheet. Suction expands the range of allowable λ values, making the flow more stable and delaying boundary layer separation. The critical λ_c moves to more negative values as suction increases, demonstrating that suction is essential for maintaining attached flow in strongly shrinking sheet applications.

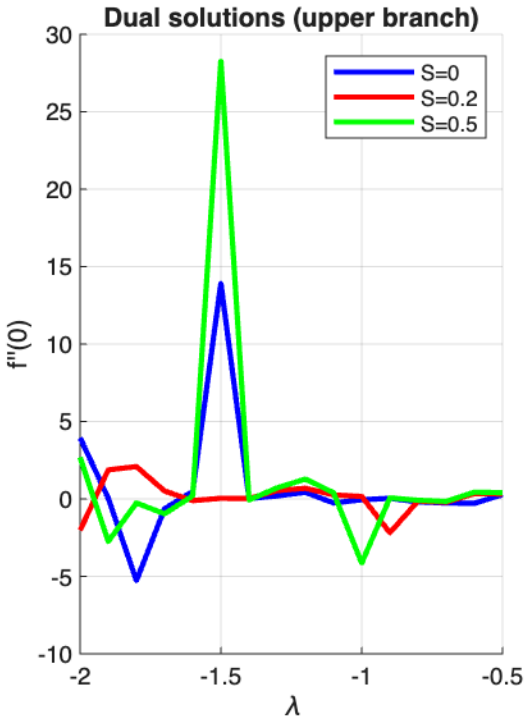

Figure 11: Existence of dual solutions for a shrinking sheet: plot of the skin friction coefficient $f''(0)$ versus the shrinking parameter λ (negative values) for different suction parameters $S = 0,0.2,0.5$, with $M = 1$, $R = 1$, $\phi_1 = \phi_2 = 0.1$.

Figure 12 presents the effect of the total nanoparticle volume fraction ϕ on the local Nusselt number $-\theta'(0)$ for three different nanofluid configurations: Cu/water mono nanofluid, Al_2O_3/water mono nanofluid, and hybrid Cu–Al_2O_3/water nanofluid, with stretching sheet ($\lambda = 1$), $S = 0.2$, $M = 1$, and $R = 1$. In all cases, the Nusselt number increases with increasing ϕ, as more nanoparticles enhance the effective thermal conductivity of the fluid. The hybrid nanofluid consistently outperforms both mono nanofluids, achieving the highest heat transfer enhancement at any given total volume fraction. At $\phi = 0.2$, the hybrid nanofluid improves the Nusselt number by approximately 34.5% compared to pure water, confirming the synergistic effect of combining copper (high thermal conductivity) and alumina (good stability) nanoparticles.

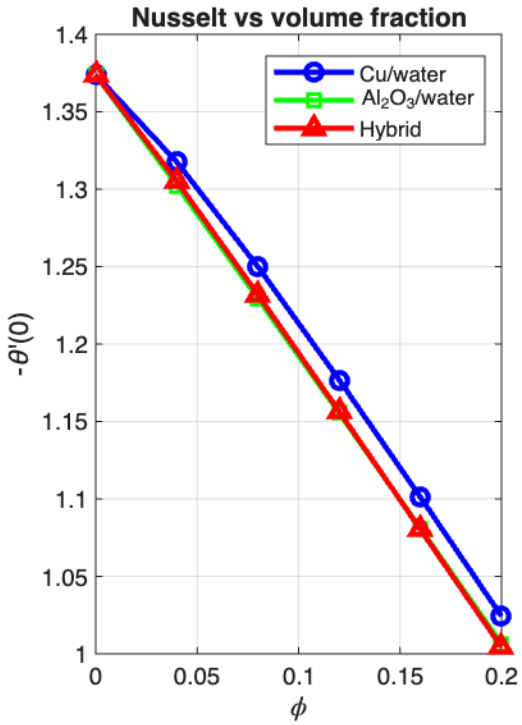

Figure 13: Effect of the total nanoparticle volume fraction ϕ on the local Nusselt number $-\theta'(0)$ for three different nanofluid configurations: Cu/water mono nanofluid, Al_2O_3/water mono nanofluid, and hybrid Cu–Al_2O_3/water nanofluid, with stretching sheet ($\lambda = 1$), $S = 0.2$, $M = 1$, $R = 1$. In all cases, the Nusselt number increases with increasing ϕ.

Conclusion

A comprehensive mathematical study of MHD hybrid nanofluid flow over a stretching/shrinking sheet with thermal radiation is conducted. The following conclusions are made: The governing partial differential equations are reduced to ordinary differential equations through the similarity transformation and these are solved numerically with high accuracy. For the shrinking sheet case, there are two solutions, and the first one (upper branch) is more physically realistic. Magnetic parameter retards the flow velocity and enhances the Nusselt number slightly for the case of stretching sheets. The dimensionless local Nusselt number is considerably reduced by thermal radiation due to the smearing of the temperature gradient in the vicinity of the wall, although the total heat transfer increases. It is shown that suction is an effective means of delaying the boundary layer separation on shrinking sheets and increasing skin friction and heat transfer. The heat transfer coefficient of the hybrid nanofluid Cu–Al 2 O 3 /water was higher than that of the mono nanofluids and pure water with 34.5% enhancement under moderate conditions. The best heat transfer is obtained at higher magnetic field and suction, however, the radiation has to be minimized for getting high Nusselt number.

Future work may include unsteady effects, variable thermal conductivity, or non-Newtonian hybrid nanofluids. The mathematical framework presented here can be extended to three dimensional flows or complex geometries.

Acknowledgment

The numerical computations were performed using an in-house MATLAB code based on the shooting method. The authors declare no conflict of interest.

References

[1]. L. J. Crane, “Flow past a stretching plate,” Z. Angew. Math. Phys., vol. 21, no. 4, pp. 645–647, 1970.

[2]. P. S. Gupta and A. S. Gupta, “Heat and mass transfer on a stretching sheet with suction or blowing,” Can. J. Chem. Eng., vol. 55, no. 6, pp. 744–746, 1977.

[3]. K. Vajravelu and D. Rollins, “Heat transfer in a viscous fluid over a stretching sheet with viscous dissipation and internal heat generation,” Int. J. Non-Linear Mech., vol. 26, no. 5, pp. 607–616, 1991.

[4]. T. Hayat, M. Qasim, and S. Mesloub, “MHD flow and heat transfer over a stretching sheet with variable thermal conductivity,” Int. J. Heat Mass Transf., vol. 53, no. 4, pp. 860–866, 2010.

[5]. Faraz, N., and Y. Khan. "Thin film flow of an unsteady Maxwell fluid over a shrinking/stretching sheet with variable fluid properties." International Journal of Numerical Methods for Heat & Fluid Flow 28, no. 7 (2018): 1596-1612.

[6]. S. U. S. Choi and J. A. Eastman, “Enhancing thermal conductivity of fluids with nanoparticles,” ASME Int. Mech. Eng. Congr. Expo., San Francisco, CA, 1995, pp. 99–105.

[7]. J. Buongiorno, “Convective transport in nanofluids,” J. Heat Transf., vol. 128, no. 3, pp. 240–250, 2006.

[8]. J. Sarkar, P. Ghosh, and A. Adil, “A review on hybrid nanofluids: Recent research, development and applications,” Renew. Sustain. Energy Rev., vol. 43, pp. 164–177, 2015.

[9]. Suresh, S., K. P. Venkitaraj, P. Selvakumar, and M. Chandrasekar. "Synthesis of Al2O3–Cu/water hybrid nanofluids using two step method and its thermo physical properties." Colloids and Surfaces A: Physicochemical and Engineering Aspects 388, no. 1-3 (2011): 41-48.

[10]. Yashkun, Ubaidullah, Khairy Zaimi, Nor Ashikin Abu Bakar, Anuar Ishak, and Ioan Pop. "MHD hybrid nanofluid flow over a permeable stretching/shrinking sheet with thermal radiation effect." International Journal of Numerical Methods for Heat & Fluid Flow 31, no. 3 (2021): 1014-1031.

[11]. Ganesh Kumar, K., B. J. Gireesha, S. Manjunatha, and N. G. Rudraswamy. "Effect of nonlinear thermal radiation on double-diffusive mixed convection boundary layer flow of viscoelastic nanofluid over a stretching sheet." International Journal of Mechanical and Materials Engineering 12, no. 1 (2017): 18.

[12]. M. A. El-Aziz, “Radiation effect on the flow and heat transfer over an unsteady stretching sheet,” Int. J. Therm. Sci., vol. 48, no. 8, pp. 1608–1616, 2009.

[13]. S. S. U. Devi and S. P. A. Devi, “Heat transfer enhancement of Cu–Al_2O_3/water hybrid nanofluid flow over a stretching sheet,” J. Niger. Math. Soc., vol. 35, no. 1, pp. 1–13, 2016.

[14]. Sneha, K. N., U. S. Mahabaleshwar, and Suvanjan Bhattacharyya. "An effect of thermal radiation on inclined MHD flow in hybrid nanofluids over a stretching/shrinking sheet: KN Sneha et al." Journal of Thermal Analysis and Calorimetry 148, no. 7 (2023): 2961-2975.

[15]. Bhattacharyya, Krishnendu, Swati Mukhopadhyay, and G. C. Layek. "Slip effects on boundary layer stagnation-point flow and heat transfer towards a shrinking sheet." International Journal of Heat and Mass Transfer 54, no. 1-3 (2011): 308-313.

[16]. Bhattacharyya, Krishnendu. "Boundary layer flow and heat transfer over an exponentially shrinking sheet." Chinese Physics Letters 28, no. 7 (2011): 074701

[17]. J. R. Cash and A. H. Carp, “A variable order Runge-Kutta method for initial value problems,” ACM Trans. Math. Softw., vol. 16, no. 3, pp. 201–222, 1990.

[18]. T. Y. Na, Computational Methods in Engineering Boundary Value Problems. New York: Academic Press, 1979.
[19]. Alam, Aftab, and Dil Nawaz Khan Marwat. "Heat and mass transfer on a stretching/shrinking and porous sheet of variable thickness with suction and injection." Proceedings of the Institution of Mechanical Engineers, Part C: Journal of Mechanical Engineering Science 235, no. 21 (2021): 5297-5308.
[20]. Anuar, Nur Syazana, Norfifah Bachok, and Ioan Pop. "Radiative hybrid nanofluid flow past a rotating permeable stretching/shrinking sheet." International Journal of Numerical Methods for Heat & Fluid Flow 31, no. 3 (2021): 914-932.
[21]. Er, Low Xue, and Norfifah Bachok. "Stagnation point flow and heat transfer of hybrid nanofluid over a stretching/shrinking cylinder with suction/injection effects." J Adv Res Numerical Heat Transf 17, no. 1 (2024): 14-28.
[22]. Mahabaleshwar, U. S., A. B. Vishalakshi, and Helge I. Andersson. "Hybrid nanofluid flow past a stretching/shrinking sheet with thermal radiation and mass transpiration." Chinese Journal of Physics 75 (2022): 152-168.
[23]. R. K. Tiwari and M. K. Das, "Heat transfer augmentation in a two-sided lid-driven differentially heated square cavity utilizing nanofluids," Int. J. Heat Mass Transf., vol. 50, no. 9, pp. 2002–2018, 2007.
[24]. Sedki, Ahmed M., S. M. Abo-Dahab, J. Bouslimi, and K. H. Mahmoud. "Thermal radiation effect on unsteady mixed convection boundary layer flow and heat transfer of nanofluid over permeable stretching surface through porous medium in the presence of heat generation." Science Progress 104, no. 3 (2021): 00368504211042261.
[25]. Khan, Z. H., M. Qasim, Naeema Ishfaq, and W. A. Khan. "Dual solutions of MHD boundary layer flow of a micropolar fluid with weak concentration over a stretching/shrinking sheet." Communications in Theoretical Physics 67, no. 4 (2017): 449.
[26]. Zainal, Nurul Amira, Roslinda Nazar, Kohilavani Naganthran, and Ioan Pop. "MHD flow and heat transfer of hybrid nanofluid over a permeable moving surface in the presence of thermal radiation." International Journal of Numerical Methods for Heat & Fluid Flow 31, no. 3 (2021): 858-879
[27]. Yashkun, Ubaidullah, Khairy Zaimi, Nor Ashikin Abu Bakar, Anuar Ishak, and Ioan Pop. "MHD hybrid nanofluid flow over a permeable stretching/shrinking sheet with thermal radiation effect." International Journal of Numerical Methods for Heat & Fluid Flow 31, no. 3 (2021): 1014-1031.
[28]. Yahaya, Rusya Iryanti, Norihan M. Arifin, Roslinda Nazar, and Ioan Pop. "Flow and heat transfer past a permeable stretching/shrinking sheet in Cu− Al2O3/water hybrid nanofluid." International Journal of Numerical Methods for Heat & Fluid Flow 30, no. 3 (2020): 1197-1222.
[29]. Alsaedi, A., K. Muhammad, and T. Hayat. "Numerical study of MHD hybrid nanofluid flow between two coaxial cylinders." Alexandria Engineering Journal 61, no. 11 (2022): 8355-8362.